Discovery of a mRNA Mitochondrial Localization Element in Saccharomyces Cerevisiae by Nonhomologous Random Recombination and In Vivo Selection

(Article begins on next page)

Discovery of a mRNA mitochondrial localization element in *Saccharomyces cerevisiae* by nonhomologous random recombination and *in vivo* selection

Jane M. Liu and David R. Liu*

Howard Hughes Medical Institute, Department of Chemistry and Chemical Biology, Harvard University, Cambridge, MA 01238, USA

ABSTRACT

In budding yeast, over 100 nuclear-encoded mRNAs are localized to the mitochondria. The determinants of mRNA localization to the mitochondria are not well understood, and protein factors involved in this process have not yet been identified. To reveal the sequence determinants for mitochondrial localization in a comprehensive and unbiased manner, we generated highly diversified libraries of 3′ UTR regions from a known mitochondrially localized mRNA by nonhomologous random recombination (NRR) and subjected the resulting sequences to an *in vivo* selection that links cell survival to mitochondrial mRNA localization. When applied to the yeast *ATP2* mRNA, this approach rapidly identified a 50-nt consensus motif, designated Min2, as well as two Min2-homologous regions naturally present downstream of the *ATP2* stop codon, which are sufficient when appended to the 3′ end of various reporter mRNAs to induce mitochondrial localization. Site-directed mutagenesis of Min2 revealed primary and secondary structure elements that contribute to localization activity. In addition, the Min2 motif may facilitate the identification of proteins involved in this mode of establishing cellular asymmetry.

INTRODUCTION

The asymmetric distribution of proteins within a cell is essential for differentiation and development. The transport of mRNAs to the site of future protein localization is an important mechanism of achieving this asymmetry (1–5). For example, studies from several groups have demonstrated that *ASH1* mRNA, along with at least 23 other transcripts, is localized to the bud tips of *Saccharomyces cerevisiae* cells (3,4,6,7). The *cis*-acting mRNA "zip-codes", as well as several *trans*-acting proteins involved in bud tip localization, have been identified and dissected at a molecular level (8–12).

In contrast, while over 100 nuclear-encoded mRNAs are localized to yeast mitochondria, much less is known about the molecular basis of their translocation (1,5,13–16). The *ATP2* transcript is one such nuclear-encoded mitochondrial mRNA. Encoding the β-subunit of the F1-ATPase, the mitochondrial localization of the *ATP2* transcript is essential for proper yeast respiratory function (15,17). Corral-Debrinski and coworkers (17) have identified a stretch of 250 nt in the 3′ UTR of *ATP2* that is sufficient for mRNA localization and allows for the biogenesis of functional mitochondria. Anderson and Parker (18) computationally identified a 10-nt (CYTGTAAATA) sequence present in the 3′ UTR of 38 nuclear genes targeted to the mitochondria; however, this sequence is not present in *ATP2*. The minimal *cis*-determinants of *ATP2* localization, and those of other nuclear-encoded mitochondrial mRNAs, remain to be determined and characterized in detail. In addition, whereas several protein factors necessary for *ASH1* mRNA transport have been characterized, no observation or identification of *trans*-acting factors involved in *ATP2* localization have yet been reported.

Nonhomologous random recombination (NRR) is a nucleic acid diversification method that generates sequences containing randomly recombined fragments of length defined by the researcher (19,20). NRR allows extensive insertion, deletion and reorientation of subsequences within a starting gene, and has recently been used to study the bud tip localization of *ASH1* (9), and to functionally dissect sRNAs and proteins in bacteria as well as *in vitro* evolved ribozymes (20–22). In this work we report the use of NRR, coupled with a simple genetic selection for localization, to identify a minimal RNA motif sufficient for targeting the *ATP2* transcript to

*To whom correspondence should be addressed. Tel: +1 617 496 1067; Fax: +1 617 496 5688; Email: drliu@fas.harvard.edu

the mitochondria. Additional mutagenesis combined with secondary structure prediction was used to functionally dissect this minimal motif, leading to the identification of elements necessary for localization activity.

MATERIALS AND METHODS

Strains

Escherichia coli strain DH10B was purchased from Invitrogen. *Saccharomyces cerevisiae* strain *ATP2-3′ADH1*, kindly provided by M. Corral-Debrinski (17), was used in the genetic selection experiments and subsequent biochemical assays. In this strain, the C-terminus of the *ATP2* ORF is fused to three tandem repeats of the influenza virus hemagglutin epitope (3HA), followed by the 3' UTR of *ADH1* (encoding a cytoplasmic protein), and the *TRP* marker. *Saccharomyces cerevisiae* strain *BY4741* (*MAT*a, *his3Δ1, leu2Δ0, met15Δ0, ura3Δ0*), purchased from ATCC, was used for fluorescent microscopy experiments. Strain *BY4741(COX4-RFP)* was constructed according to previously published protocols using plasmid pFA6a-link-tdimer2-Ura3, kindly provided by K. Thorn and R. Tsien (23,24).

Plasmid preparation

Plasmid pRSAM3 was the generous gift of Professor M. Corral-Debrinski (17) and contains a 2.5-kb fragment containing the *ATP2* promoter, ORF and full-length 3' UTR (636 bp) inserted into pRS416 between the SalI and EcoRI sites. Plasmid pATP2 was created as follows: DNA oligonucleotides OA and OB were annealed, digested with EcoRI and SmaI and inserted into pre-digested pRSAM3 to introduce the library cloning site BstEII (GGTGACC), resulting in plasmid pRSAM3–B. Primers PA and PB were used in a PCR reaction to generate a 1.8-kb fragment containing the *ATP2* promoter, *ATP2* ORF and 13-bp of the 3' UTR. This fragment was introduced into the SalI and BstEII sites of pRSAM3-B to generate pRSAM3-C. To facilitate cloning, a second BstEII (5′-GGTAACC) was introduced 550 nt downstream of the first BstEII site by quick-change mutagenesis, affording the final selection plasmid pATP2. The original pSAM3 and *S. cerevisiae* genomic DNA (Novagen) were used as PCR templates for amplifying regions of the *ATP2* and *ATM1* 3' UTRs, respectively, to create control plasmids pATP2-636, pATP2-250 and pATP2-ATM1.

Plasmids pT220 and gRNA were generous gifts of Prof. J. DeRisi (6). Plasmid pT220, carrying *TRP* and AmpR markers, expresses a U1A RNA-binding protein as a fusion with GFP. Plasmid gRNA, carrying *HIS* and AmpR markers, expresses four tandem repeats of the U1A RNA hairpin (6,12) followed by a NotI cloning site. Two BstEII cloning sites (5′-GGTGACC and 5′-GGTAACC) were introduced into the NotI site to simplify cloning.

Sequences of oligonucleotides used above are as follows (restriction sites in italics):

OA: 5′-GCC*GAATTC*ACGGGTGACCATGAC*CCCGGG*GGCGGC

OB: 5′-GCCGCC*CCCGGGG*TCATGGTCACCCGT*GAATTC*GGC

PA: 5′-GGCGGC*GTCGAC*CTTAGATACAACGCTTATAAAGAACGC

PB: 5′-GCCGCC*GGTCACC*AGCTTTATTTCTTCTAGTTGGCTTCAG

636for: 5′-GGCGGC*GGTGACC*TAGAAGAAATAAAGCTTAAACCAAGG

636rev: 5′-GGCGGC*GGTTACC*ACATGTCCAGTGGGAAAGCG

250for: 5′-GGCGGC*GGTGACC*TAGAAGAAATAAAGCTTAAACCAAGG

250rev: 5′-GGCGGC*GGTTACC*CTTTATTTACTTACAGTTGGGAGTAAA

ATM1for: 5′-GGCGGC*GGTGACC*TGAACGCTCGTAAGTAAATATTG

ATM1rev: 5′-GGCGGC*GGTTACC*CCGAGTGGTTTGGTTTGCTAATAC

Construction of NRR-diversified *ATP2* 3′ UTR libraries

Using pATP2–636 as a template, the 3′ UTR of *ATP2* was amplified by PCR with primers PC and PD. NRR was performed on the resulting PCR products as previously described (19,20). HPA and HPB contain BstEII sites (italics) for ligation into the selection plasmid pATP2; they also contain PvuII sites (underlined) for removal of hairpin ends and both end with AgeI half-sites (ACC/GGT) for digesting hairpin dimers. Recombined genes were amplified by PCR using primers PE and PF, and the resulting products were digested with BstEII. The desired size range of recombined DNA was purified by gel electrophoresis then ligated into pATP2 to generate the corresponding NRR-diversified library.

Sequences of oligonucleotides used above are as follows:

PC: 5′-pAAGAAATAAAGCTTAAACCAAGGGAAGC

PD: 5′-pACATGTCCAGTGGGAAAGCGAGG

HPA: 5′ p*GGTCACC*CATCCGAATT<u>CAGCTG</u>GCGGCGGCCGCCGCC<u>CAGCTG</u>AATTCGGAT*GGGTGACC*

HPB: 5′-p*GGTAACC*CATCCGAATT<u>CAGCTG</u>GCGGCGGCCGCCGCC<u>CAGCTG</u>AATTCGGATG*GGTTACC*

PE: 5′-CTGAATTCGGATG*GGTGACC*

PF: 5′-CTGAATTCGGATG*GGTTACC*

Construction of random 60-nt library

Primers PG and PH (250 pmol each) were annealed and extended with Klenow DNA polymerase (NEB). The resulting random DNA library was digested with BstEII, then purified by gel electrophoresis and ligated into pATP2.

Sequences of oligonucleotides used above are as follows:

PG: 5′-GGC*GGTGACC*(N$_{60}$)*GGTAACC*GCGGCCGC

PH: 5′-GCGGCCGC*GGTTACC*

Selection for mRNA mitochondrial localization

DH10B cells were transformed with pATP2 libraries generated as described above, yielding initial library

complexities of 5×10^7 to 2×10^8 transformants. The plasmid library was amplified in DH10B cells in 300 ml $2 \times$ yeast-tryptone ($2 \times$ YT) + 100 μg/ml carbenicillin (Cb), then transformed into *S. cerevisiae* strain *ATP2-3'ADH1* (10^3–10^5 transformants). The yeast library was grown in YPD medium containing 3% glucose and plated on 2% glycerol complete synthetic medium lacking tryptophan and uracil (-trp -ura). After 2–3 days at 30°C, colonies were picked and regrown on selective medium. After 36 h at 30°C, survivors were grown in 3% glycerol medium (-trp -ura). Plasmids were isolated from cultures that showed growth after 2 days at 30°C. The random 60-nt library (initial complexity of 4×10^7) was similarly transformed into *ATP2-3'ADH1* (6×10^5 transformants) and selected for the ability to induce mRNA localization.

The 3'-UTR insert of surviving colonies was amplified by PCR using primers PH and PI. Amplified products were digested with DpnI, then with BstEII. The digested fragments were purified by gel electrophoresis or using QIAquick spin columns (Qiagen), then introduced into BstEII-digested pATP2 or gRNA.

Sequences of oligonucleotides used above are as follows:

PH: 5′-GCGGCCGC*GGTTACC*
PI: 5′-GAAGAAATAAAGCT*GGTGACC*

Minimal sequence generation

All minimal motifs and mutants thereof were made by annealing 300 pmol of overlapping DNA oligonucleotides (Integrated DNA Technologies) that has been first 5′-phosphorylated using T4 polynucleotide kinase (NEB). Annealed fragments were introduced directly into BstEII-digested pATP2 or gRNA.

Cell microscopy

For visualization of RNA, the gRNA plasmid carrying the RNA of interest was introduced into *BY4741* or *BY4741(COX4-RFP)* cells harboring pT220 (i.e. expressing U1Ap-GFP). Cells were grown overnight in complete synthetic medium lacking histidine and tryptophan (-his -trp), with 2% raffinose as the carbon source. The next morning, 200–250 μl of dense culture was harvested by centrifugation and re-suspended in 1 ml of low-fluorescent medium (23) (LF -his-trp) supplemented with 2% glycerol. Cells were grown for 2 h at 30°C, induced with galactose (to 0.2%) and allowed to grow for another 2 h, at which point 0.2 μl MitoTracker Red CHXRos (1 mM, Molecular Probes) was added for an additional 20 min. Cells were pelleted, washed twice with LF -his -trp, re-suspended in LF medium with glycerol and immobilized on concanavalin A-coated coverslips for imaging (23). When strain *BY4741(COX4-RFP)* was used, cells were visualized directly after 2.5 h of galactose induction.

The following excitation/emission pairs (in nanometer) were used: GFP, 476/512; RFP (tdimer2), 552/579; MitoTracker Red CMXRos, 579/599. Microscopy was performed on a Zeiss Axio Imager M1 with either a $63 \times /1.4$ NA oil-immersion (Figure 4A) or a $100 \times /1.4$ NA oil-immersion objective (Figure 4B). Images were recorded on a Zeiss Axiocam MRm with 2×2 binning, and processed using Axiovision software (Zeiss). On average, >50 individual cells per strain were visualized and scored for GFP localization to the mitochondria. The images shown in Figure 4 are representative examples of each strain analyzed.

RNA isolation

ATP2-3'ADH1 cells harboring pATP2 expressing the RNA of interest were grown to mid-log phase. Total RNA was isolated using the RiboPure-Yeast Kit (Ambion) according to the manufacturer's protocol. RNA samples for quantitative reverse transcriptase PCR (qRT-PCR) experiments were treated further with 2 U DNase I (NEB), for a total of 2 DNase treatments. For mRNA decay analysis, 3 μg/ml thiolutin (Sigma) was added to mid-log-phase cells, and culture samples were removed, centrifuged and frozen after 0–100 min of drug exposure (25); total RNA was then extracted as above.

Poly(A) RNA was isolated from cells grown to mid-log-phase following the protocol provided by J. DeRisi (http://derisilab.ucsf.edu). Briefly, total RNA was isolated from cells using hot acid phenol. The aqueous supernatant was poured into prespun 50 ml Phase Lock Gel tubes (Eppendorf). An equal volume of chloroform was added and the tubes spun at 3000 r.p.m. for 10 min. Following ethanol precipitation, 2 mg of RNA was denatured (65°C, 10 min) and incubated with 75 mg oligo dT cellulose (Amersham Biosciences) for 1 h at RT. The RNA/cellulose mixture was washed with $1 \times$ NETS (0.6 M NaCl, 10 mM EDTA, 10 mM Tris, pH 7.4, 0.2% SDS). Finally, the RNA was eluted with $1 \times$ ETS (10 mM EDTA, 10 mM Tris, pH 7.4, 0.2% SDS) and ethanol-precipitated.

Northern blotting analysis

Northern blots were performed following the protocol provided with the Odyssey Infrared Imaging System (LI-COR Biosciences). Briefly, RNA sample loading buffer (Sigma) was added to 5 μg total RNA. Samples were incubated at 65°C, 10 min, placed on ice, then run on denaturing 1.3% agarose gels in $1 \times$ MOPS running buffer (Ambion) for 70 min at 80 V. Samples were transferred onto Odyssey nylon membranes (LI-COR Biosciences) using the NorthernMax Kit (Ambion). RNA was cross-linked to the membrane (UVC 515 Ultraviolet Mutlilinker, UltraLum); the blot was pre-hybridized at 42°C with ULTRAhyp-Oligo Buffer (Ambion). Blots were hybridized overnight at 42°C with biotinylated probes and then washed with Low and High Stringency Washes (Ambion). Blots were blocked for 30 min with Odyssey Blocking Buffer plus 1% SDS (LI-COR Biosciences) and then incubated for 30 min with Streptavidin IRDye 800 CW conjugate in blocking buffer plus 1% SDS (LI-COR Biosciences). Blots were washed three times with $1 \times$ PBST, one time with $1 \times$ PBS then scanned on an Odyssey IR Imaging System (LI-COR Biosciences).

To generate biotinylated probes, pATP2-636 or *S. cerevisiae* genomic DNA was used as a template for the PCR amplification in the presence of biotin-16-dUTP (2:3 biotin-dUTP:TTP, Roche). The probe for yeast *ACT1*

mRNA is a PCR-amplified 0.5 kb coding sequence, and the probe for *ATP2* mRNA is 150 bp extending from the coding sequence into the first BstEII cloning site of pATP2.

qRT-PCR

Total RNA was isolated as described above and 1 µg RNA was treated with MMLV–reverse transcriptase (MMLV–RT, NEB) at 42°C for 1 h in the presence of primer PJ (*ATP2*-specific) or PK (*ACT1*-specific). MMLV–RT activity was terminated by heating at 92°C for 10 min. Serial dilutions of purified and quantified pATP2–636 or *S. cerevisiae* genomic DNA (Novagen) were used as reference templates to facilitate the accuracy of comparisons between RNA samples during qPCR. The reference DNA or 1 µl of the MMLV–RT reaction was mixed with 25 pmol of sense (PL, *ATP2*; PM, *ACT1*) and reverse primers (PJ; PN, *ACT1*), 2 × QuantiTect SYBR Green PCR Master Mix (Qiagen) and nuclease-free water to a final volume of 50 µl. Quantitative PCR reactions were performed using a DNA Engine Opticon 2 (MJ Research) with an initial denaturation step of 15 min at 95°C followed by 40 cycles of 30 s at 94°C, 45 s at 56°C and 45 s at 72°C. The fluorescence was measured at the end of each extension step. Finally, a melting curve was recorded between 48°C and 99°C with a hold ever 2 s. Relative RNA concentrations were calculated by comparison to the standard curves; amounts of *ATP2* mRNA were standardized to *ACT1* mRNA. Control reactions were performed for each run and included samples not treated with MMLV–RT or samples lacking template RNA; no signal was observed in these control cases.

Sequences of oligonucleotides used above are as follows:

PJ: 5′-GGTCACCAGCTTTATTTCTTCTAGTTG

PK: 5′-TTAGAAACACTTGTGGTGAACGATAGATG

PL: 5′-CGTTCAAAGCCGTTTTGGAAGG

PM: 5′-ATTGCTCCTCCAGAAAGAAAGTACTC

PN: 5′-GTGAACGATAGATGGACCACTTTC

RESULTS

Selection system for mRNA mitochondrial localization

Our approach requires a method for rapidly evaluating the mitochondrial localization of a large number of mRNA variants. Corral-Debrinski and colleagues (17) previously reported that when the 3′ UTR of endogenous *ATP2* was replaced by the 3′ UTR of the transcript encoding the cytoplasmic protein Adh1p, the resulting strain (designated *ATP2-3′ADH1*) displayed respiratory dysfunction and was unable to grow on media in which glycerol was the sole carbon source. Expressing *ATP2* with its wild-type 3′ UTR from a plasmid rescued cell growth on glycerol media. Fractionation experiments conducted by Corral-Debrinski and coworkers (17) further demonstrated that the respiratory dysfunction was a result of abnormal localization of the *ATP2-3′ADH1* mRNA, which was predominantly localized to cytoplasmic polysomes, rather than mitochondrion-bound
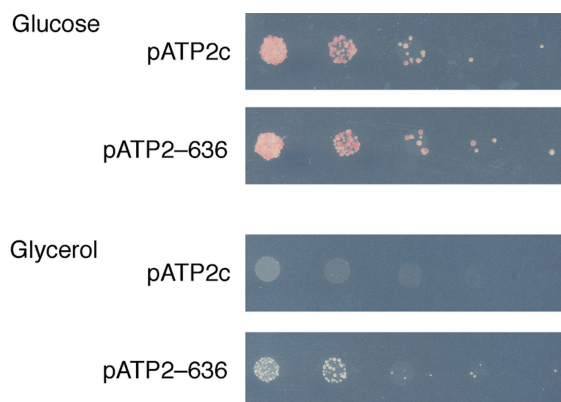
Figure 1. Validation of an *in vivo* selection for mRNA mitochondrial localization (17). Plasmid pATP2 expressing either a negative control 3′ UTR (pATP2c) or the wild-type *ATP2* 3′ UTR (pATP2-636) was introduced into strain *ATP2-3′ADH1*. Ten-fold serial dilutions of the resulting strains were plated on media (-trp -ura) under either nonselective conditions (with glucose as the sole carbon source, top) or selective conditions (with glycerol as the sole carbon source, bottom).

ones. Corral-Debrinski and coworkers (17) also provided evidence that expression of *ATP2* from a plasmid with either its full-length 3′ UTR, or with the first 250 nt of its wild-type 3′ UTR, resulted in *ATP2* mRNAs accumulating on mitochondrion-bound polysomes.

Based on these compelling results, we reasoned that survival on glycerol minimal media, coupled with other screens for mitochondrial mRNA localization, could serve as an effective system to rapidly assay RNA sequences for mitochondrial localization activity. We therefore developed the previous findings of Corral-Debrinski and coworkers into a simple selection system to study localization elements that direct nuclear-encoded mRNAs to the mitochondria. In this selection, *ATP2-3′ADH1* cells harbor the plasmid pATP2, which expresses *ATP2* from its native promoter with a library of 3′ UTR sequences immediately downstream of the *ATP2* stop codon. Only in the presence of *ATP2* transcripts bearing 3′ UTRs that enable mitochondrial localization should cells be able to grow on glycerol media.

This selection method was validated by introducing into *ATP2-3′ADH1* cells plasmid pATP2 expressing either the full-length *ATP2* 3′ UTR (pATP2–636), an active, shortened *ATP2* 3′ UTR (first 250 nt; pATP2-250) (17) or a random 500 nt 3′ UTR (pATP2c). The full-length 3′ UTR from *ATM1*, another nuclear-encoded mitochondrial protein, was used as an additional positive control (pATP2-ATM1) (26). When plated on synthetic medium containing glycerol, a survival rate of only 0.05% was observed in cells carrying the random 3′ UTR plasmid, pATP2c (Figure 1). In contrast, when either of the two *ATP2* 3′ UTR variants (636 or 250 nt) or the *ATM1* 3′ UTR was expressed, >50% of the cells plated survived on glycerol medium (Figure 1 and data not shown). These results suggest that the above selection successfully links cell survival with having localization-competent 3′ UTRs in a manner that does not rely on *ATP2*-specific 3′ UTR elements.

To verify mitochondrial localization of clones surviving the selection, we used the 'green-RNA' system previously described by Vale and coworkers (6,12) for visualizing mRNA localization *in vivo*. In the green-RNA system, RNAs are transcriptionally fused to a U1A RNA hairpin (U1Ahp), which is bound by the U1A-binding protein (U1Ap). U1Ap, in turn, is translationally fused to GFP. Mitochondria were labeled with the rhodamine-derived, mitochondrion-specific dye, MitoTracker (MT, Molecular Probes) or with endogenously expressed Cox4p-RFP fusion proteins (23,27) (see Materials and Methods section). Colocalization of GFP–RNA complexes with either MT or Cox4p-RFP suggests RNA localization to the mitochondria. In this work, RNA sequences that could both survive the selection described above and localize GFP–RNA complexes to the mitochondria were considered functional 3′ UTRs.

Creation of NRR-diversified libraries

The NRR method (19,21) was used to diversify the full-length 3′ UTR of *ATP2* (636 bp) into three libraries (L1, L2 and L3) of randomly and nonhomologously recombined fragments. The average length of each recombining fragment, as well as the average total length of each recombined library member, was controlled (19) to dissect the UTR at different resolutions and to maximize the likelihood of finding minimal active motifs. In library L1, blunt-ended 30–200 bp 3′ UTR fragments were recombined into 200–400 bp 3′ UTRs. Library L2 was generated by recombining 30–50 bp fragments into 150–400 bp 3′ UTRs. Finally, 40–100 bp fragments were joined into 100–150 bp recombinants in library L3. Each library was cloned into pATP2 and introduced into *E. coli* DH10B cells, generating libraries of 5×10^7 to 2×10^8 transformants. For comparison, we also prepared library N1, expressing 60 consecutive random RNA nucleotides (4×10^7 transformants).

To assess the diversity introduced by NRR, 19 library members from L1 to L3 were characterized by DNA sequencing prior to any functional selection (Figure 2). The composition of the diversified library members was observed to be consistent with the library design parameters. For example, the characterized sequences from L1 averaged 215 bp in length and contained up to five crossovers, between fragments ranging in size from 14 to 300 nt. Similarly, the characterized sequences from L3 averaged 100 bp in length and contained up to four crossovers, between fragments ranging in size from 18 to 54 bp.

### Selection and mutagenesis of functional *ATP2* 3′ UTRs

The three NRR-diversified 3′ UTR libraries were each introduced into yeast cells, and the resulting transformants were selected for their ability to localize the *ATP2* mRNA to the mitochondria as described above. For each of the three NRR-based libraries, we observed that 1 in ~250 transformants (from 10^5 total transformants) were able to survive under selective conditions, regardless of the library construction method. A subset of surviving colonies was further characterized by subcloning their
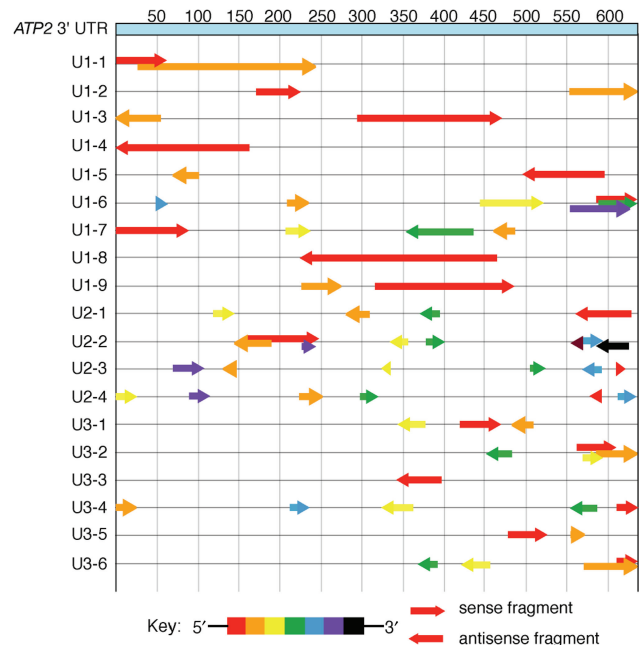
Figure 2. Composition of NRR-diversified *ATP2* 3′ UTR variants before selection. The numbering across the top of the figure corresponds to the nucleotide position in the 3′ UTR of *ATP2*, where '1' is the first nucleotide immediately after the stop codon. Each arrow represents an *ATP2* fragment. Arrow positions indicate the origin of each fragment within the parental *ATP2* gene. Arrow colors indicate the order of the fragment reassembly (5′-red-orange-yellow...black-3′, as shown at the bottom of the figure). The direction of each arrow identifies whether the fragment came from the sense (pointing right) or antisense (pointing left) strand of *ATP2*. The clone names beginning with 'U1', 'U2' and 'U3' came from library L1, L2 and L3, respectively.

UTR inserts into fresh pATP2, followed by reselection to confirm their activity. In total, 45 clones from L1 to L3 were characterized as exhibiting growth phenotypes under selective conditions consistent with mitochondrial localization of *ATP2* mRNA (Figure 3). Among these 45 sequences, 14 were characterized by fluorescence microscopy using the green-RNA system, of which 13 (92%) were observed to colocalize with MitoTracker (Figure 4A; clone 4–53 failed to colocalize with MT, data not shown). The high degree of correspondence between the selection phenotypes and the corresponding green-RNA observations is consistent with the basic assumption that the selection system enriches library members with mitochondrial localization activity.

The random (N1) library, in contrast, yielded only one active clone (N1–2) out of 6×10^5 transformants subjected to selection. The much lower frequency of active sequences in the random RNA library suggests that the survivors isolated from the *ATP2* mRNA-based library derive their activity from sequence elements present within the natural mRNA, rather than from the chance construction of unrelated, but active, sequences through random recombination. In addition, the very low survival rate of cells expressing the N1 library indicates that 60 nt mitochondrially localizing UTRs appear only very rarely within random RNA sequence space.
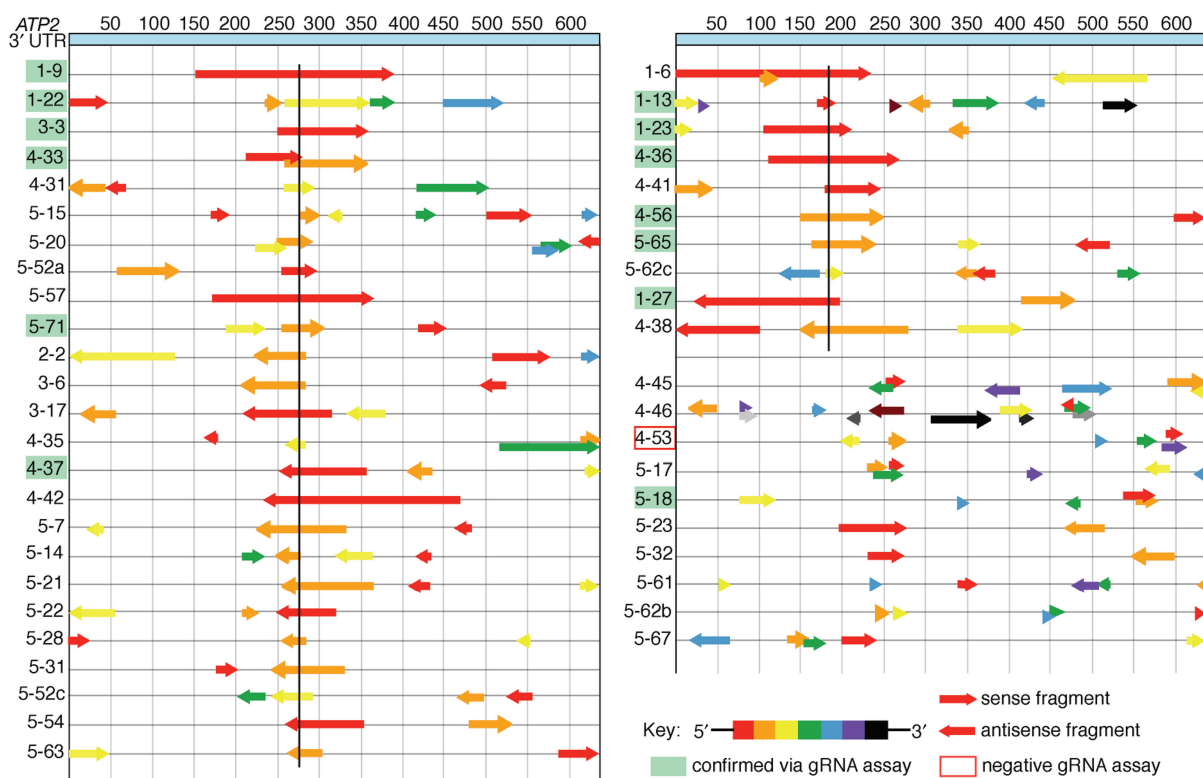
Figure 3. Composition of 3′ UTR variants surviving selection for mitochondrial localization. Sequences shown are able to localize *ATP2* mRNA to the mitochondria, as determined by their ability to rescue *ATP2-3′ADH1* cell growth on glycerol media when expressed from pATP2. The labeling scheme is as described in Figure 2. The 14 variants highlighted in green and red were also screened with the green-RNA system; the 13 variants boxed in green were able to localize GFP-labeled *ATP2* mRNA to the mitochondria, while 4–53 did not localize gRNA-particles to the mitochondria (see text and Figure 4). Vertical black lines indicate fragments that run through one of the two regions of the *ATP2* 3′ UTR (nt 263–312 and nt 164–213) that share homology with minimal localization motif Min2.

Within the 45 active sequences, two regions of the *ATP2* 3′ UTR are strongly overrepresented (Figure 3). The first region is 250–300 nt downstream of the *ATP2* stop codon (Figure 3). The second region, 150–200 nt after the stop codon, is present in a smaller fraction of the active 3′ UTR variants, but is still significantly overrepresented (Figure 3). Out of the 13 variants that were active in the green-RNA screen, 12 (92%) contain either one or both of these two regions.

In order to further pinpoint active localization elements, mutants of eight multi-fragment sequences (1–23, 1–27, 4–33, 4–35, 4–37, 4–53, 4–56 and 5–28) were generated by cloning individual fragments into pATP2 and assaying for localization both by growing cells on glycerol medium and by using the green-RNA screen. Table 1 lists the original clones and the truncated mutants generated, along with their observed phenotypes. Consistent with the distribution of fragments in the active clones, the active truncated mutants contained fragments derived from one of two regions of the *ATP2* 3′ UTR centered 180 nt or 275 nt into the *ATP2* 3′ UTR. Surprisingly, several active fragments, such as 4–37A, were derived from the antisense strand of *ATP2*. The antisense strands of 4–33A and 4–33B, moreover, were also active in both the glycerol and gRNA screen (data not shown). These observations suggests that for at least some active RNA elements, secondary structure, rather than specific sequences, is sufficient to impart localization activity.

Identification and characterization of a minimal sequence motif

The single N_{60}-derived active sequence (N1-2), as well as twelve active sequences obtained from the above studies on sequences emerging from the *ATP2*-derived library (1–9, 1–13, 1–22, 1–23A, 1–27A, 4–33A, 4–33B, 4–36, 4–37A, 4–56B, 5–65, 5–71), were subjected to a Multiple Em for Motif Elicitation (MEME) sequence analysis in order to identify sequence similarities (28).

These clones were chosen for the following reasons: first, they provided a range in sequence length, ranging from 60 to 238 nt; second, they collectively represented random-derived, sense-derived and antisense-derived active sequences; lastly, these sequences exhibited positive phenotypes in both the glycerol and gRNA screens. The full-length sequences of all 13 samples are listed in Table 2. The MEME analysis identified motifs commonly found in active clones. One conserved motif, a 50-nt sequence designated Min2 (Figure 5), emerged as having by far the greatest statistical significance (lowest probability of arising randomly). The sequence logo of Min2, depicting the relative contribution of each of the original
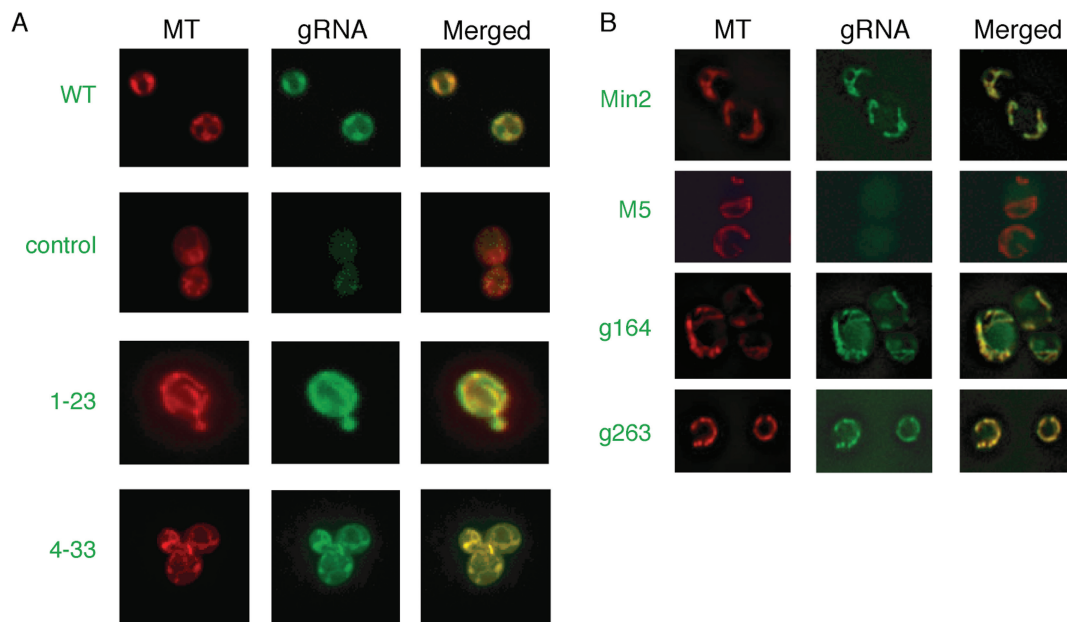
Figure 4. Visualization of mRNA mitochondrial localization. (**A**) Selected NRR variants were assayed for colocalization of GFP-linked mRNA and mitochondria-specific fluorophores, compared to positive (WT) and negative controls. WT = 636 nt *ATP2* 3′ UTR; control = random 500 nt sequence. (**B**) Minimal motifs and mutants assayed in green-RNA screen. MT = visualization corresponding to MitoTracker CMRox stain or Cox4p-RFP proteins; gRNA = visualization corresponding to GFP fluorescence emission. See Materials and Methods section.

Table 1. Analysis of variant *ATP2* 3′ UTR sequences[a]

Original clone	Glycerol[b]	gRNA[c]
1–23	+ +	+ +
1–23A	+ +	ND
1–27	+ +	+ +
1–27A	+ +	+ +
1–27B	−	ND
4–33	+ + +	+ +
4–33A	+ + +	+ +[d]
4–33B	+ + +	+ +[d]
4–35	+ +	ND
4–35ABC	−	ND
4–35AC	+ +	ND
4–35BC	−	ND
4–35C	−	ND
4–37	+ +	+ +
4–37A	+ + +	+ +
4–53	+ +	−
4–53AB	−	ND
4–53B	−	ND
4–56	+ +	ND
4–56B	+ + +	+ +
5–28	+ +	ND
5–28B	−	ND
5–28BC	+ +	ND

[a]Letters following clone number indicate fragment(s) of original clone used to generate mutants. For example, 1–23A consists of the first fragment of clone 1–23; 4–35ABC consists of the first three fragments of clone 4–35.
[b]Ability of 3′ UTR sequence, when expressed from plasmid pATP2, to rescue growth of *ATP2-3′ADH1* cells on glycerol medium.
[c]Ability of 3′ UTR sequence to colocalize gRNA-particles with MT.
[d]Antisense strand of these mutants were also able to colocalize with MT in the gRNA screen.
ND, not determined.

13 sequences towards generating the minimal motif, is depicted in Figure 6 (29,30).

Min2 variants are present twice downstream of the *ATP2* stop codon: once at nt 164–213 after the *ATP2* stop codon, and once again at nt 263–312. The first region has 36 nt out of 50 (72%) identical to Min2; whereas the second region shares 84% sequence identity (42 out of 50 nt) with Min2. The region between nt 263 and 312 induces a strong mRNA localization phenotype; when introduced as a 3′ UTR in pATP2, this region is able to rescue growth of *ATP2-3′ADH1* cells on glycerol medium ($94 \pm 4\%$ survival). The region with lower homology to Min2 (nt 164–213) was able to modestly rescue *ATP2-3′ADH1* cell growth when introduced into pATP2 ($9 \pm 2\%$ survival). Both endogenous regions of the *ATP2* 3′ UTR, however, are capable of localizing GFP-labeled RNA to the mitochondria as visualized in the green-RNA screen (Figure 4B, g164 and g263). When constructed synthetically and expressed in the 3′ UTR of *ATP2* mRNA, Min2 minimal motif itself, although not naturally present in the yeast genome, was also able to rescue *ATP2-3′ADH1* growth on glycerol medium to an extent comparable to that of wild-type *ATP2*. Min2 was also able to localize its RNA as a complex with GFP to mitochondria in the green-RNA screen (Figure 4B).

Analysis and mutagenesis of Min 2

To further understand the Min2 elements that contribute towards its localization activity, we screened a series of Min2 mutants generated by site-directed mutagenesis for localization activity using both the glycerol and green-RNA screens described above. Secondary structure prediction using the mfold algorithm (31,32) predicted

Table 2. Sequences of clones used for MEME analysis

| Clone	Sequence (5′ to 3′)
N1–2	TAATGTGTCGCGTATATACCGAAATCGTAAATATGAAATACGACTTATAGTACTTGATGC
1–9	TATCCTATTGATATTTTCTTTATATTCACTAAAAAAAAAATTTATTCTATAAGACTGACTATAATTTTTTTTAC TCCCAACTGTAAGTAAATAAAGACTCACCTACGCATACATTTTTTATATATACTATAAGATGTAGGATCTT AAAGAAAAATAAAGAGAAAAAGAGAAGCACACAACCTGCGATAAGTTGTAAGTTTGCCTCAACAGCTAT TCTACTCACTTTTTGTATCTTCGGT
1–13	TATATTCACTAAAAAAAAAATTTTATTTTTCTTTAAGATCCTACATCTAAGAAATAAAGCTTAAACCAAGGG AGCGATAAGTTGTAAGTTTGCCTCAACAGCTATTCTACTCACTTTTTGTATCTTCGGTTCACGTAATCGCA TGTGCGAAAGTGAGCAAAATTTGAATACGCATACATTTTTTATATACTTTCACATATCATGGTAGCTGTT TTAATTACCATTCTATTA
1–22	AAGAAATAAAGCTTAAACCAAGGGAAGCAAAATTGAAATACCGAAAGTAAATAAAGACTCACATACAT TTTTTATATATACTATAAGATGTAGGATCTTAAAGAAAAATAAAGAGAAAAAGAGAAGCACACAACCTGC GATAAGTTGTAAGTTTGCCTCAACAACTATTCTACTCACTTTTTGTATCTTCGGTTAACCCCTGATTTTCT TTCTGTATTAGCGTATGGCTGACTAATATTCACTTGGGGTCAACATAACTTACTTTCAC
1–23A	TCCTTCTTGTTTATTGGTATTATTATGTTACGATATTCATTCATTATCCTATTGATATTTTCTTTATATTCAC TAAAAAAAAAATTTATTCTATAAGACTGACTATA
1–27A	GAATAAATTTTTTTTTAGTGAATATAAAGAAAATATCAATAGGATAATGAATGAATATCGTAACATAATA ATACCAATAAACAAGAAGGAAGCAGGGAAAAACAAAAAAAAAAAATTATCTTTTTTTTCCCATCATCCTTA TTGTTCTACCTTCGGTATTTCAAATTTTGCTTCC
4–33A	TAATTTTTTTTACTCCCAACTGTAAGTAAATAAAGACTCACCTACGCATACATTTTTTATATATACTA
4–33B	CATACATTTTTTATATATACTATAAGATGTAGGATCTTAAAGAAAAATAAAGAGAAAAAGAGAAGCACAC AACCTGCGATAAGTTGTAAGTTTGCCTC
4–36	TTGTTTATTGGTATTATTATGTTACGATATTCATTCATTATCCTATTGATATTTTCTTTATATTCACTAAAAAA AAAATTTATTCTATAAGACTGACTATAATTTTTTTTACTCCCAACTGTAAGTAAATAAAGACTCACCTACGC ATACATTTTTTA
4–37A	GAGGCAAACTTACAACTTATCGCAGGTTGTGTGCTTCTCTTTTTCTCTTTATTTTTCTTTAAGATCCTACAT CTTATAGTATATATAAAAAATGTATGCGTAG
4–56B	TATCCTATTGATATTTTCTTTATATTCACTAAAAAAAAAATTTATTCTATAAGACTGACTATAATTTTTTTTAC TCCCAACTGTAAGTAAATAAAGACTCA
5–65	TGTGAAAGTAAGTTATGTTGACCCCAAGTGAATATTAGTCAGCCTATTTTCTTTATATTCACTAAAAAAAAA ATTTATTCTATAAGACTGACTATAATTTTTTTTACTCCCAACTGTAAGTATGTAAGTTTGCCTCAACAGCTA TTCT
5–71	CACTTTCGCACATGCGATTACGTGTATTACCCTCATACATTTTTTATATATACTATAAGATGTAGGATCTTA AAGAAAAATAAAATTTATTCTATAAGACTGACTATAATTTTTTTTACTCCCAACTGTA

that Min2 may adopt the bulged stem-loop structure depicted in Figure 5. Although not identical in sequence to Min2, the natural Min2-like region in the *ATP2* 3′ UTR (nt 263–312) is also predicted to adopt a similar secondary structure containing a long oligo U-oligo A stem and a large bulge in the middle of the folded structure (data not shown). These similarities suggest a possible biological relevance of the predicted Min2 structure.

A series of 23 site-directed mutants of Min2 were constructed and assayed for their ability to rescue *ATP2-3′ADH1* cell growth on glycerol medium. Removal of the bulge (mutant M5) abolished localization activity (Figures 4B and 5). Point mutations within this single-stranded region were also deleterious, leading to a 9.3-fold decrease in localization efficiency as measured by selection survival rates (M14). Additionally, the changes in activity resulting from complementary sets of mutations support the predicted Min2 structure (Figure 5). The top of the AU-rich stem (nt 8–10) was mutated to the sequence of the opposing strand (M22). The resulting mutant was only 13% as active as the wild-type 3′ UTR. Restoration of the predicted stem structure by introducing three compensatory base changes in the opposite strand, however, rescued localization activity to over 60% wild type (M23). The AU-rich nature of the putative stem region is important for activity, as mutation of three consecutive U:A or U:G pairs to C:G pairs resulted in no localization activity (M16). The U-rich nature of the 5′ arm of the stem and the A-rich nature of the 3′ arm are also important, as inverting the AU pairs in M20 and M23 abolished and impaired localization, respectively. Although swapping AU pairs near the terminus of the predicted stem was tolerated (M8), the 4 nt at the 5′ end and the 12 nt at the 3′ end are absolutely required for activity (M12 and M13). Taken together, these findings suggest that the both the secondary structure and the primary sequence of Min2 are involved in the mitochondrial translocation of *ATP2* mRNA. In some cases, such as those revealed by M4, M14 and M18, specific nucleotides identities are required, perhaps because of base-pairing to other regions of the *ATP2* transcript or because of binding to a protein target involved in the localization pathway (see below). In other cases, such as at the top of the AU-rich stem, base pairing but not a specific nucleotide sequence is required for activity.

Intracellular RNA expression levels and stability

To further characterize sequences emerging from selection, we probed mRNA levels of the *ATP2* mRNA and a representative set of Min2 variants by northern blot
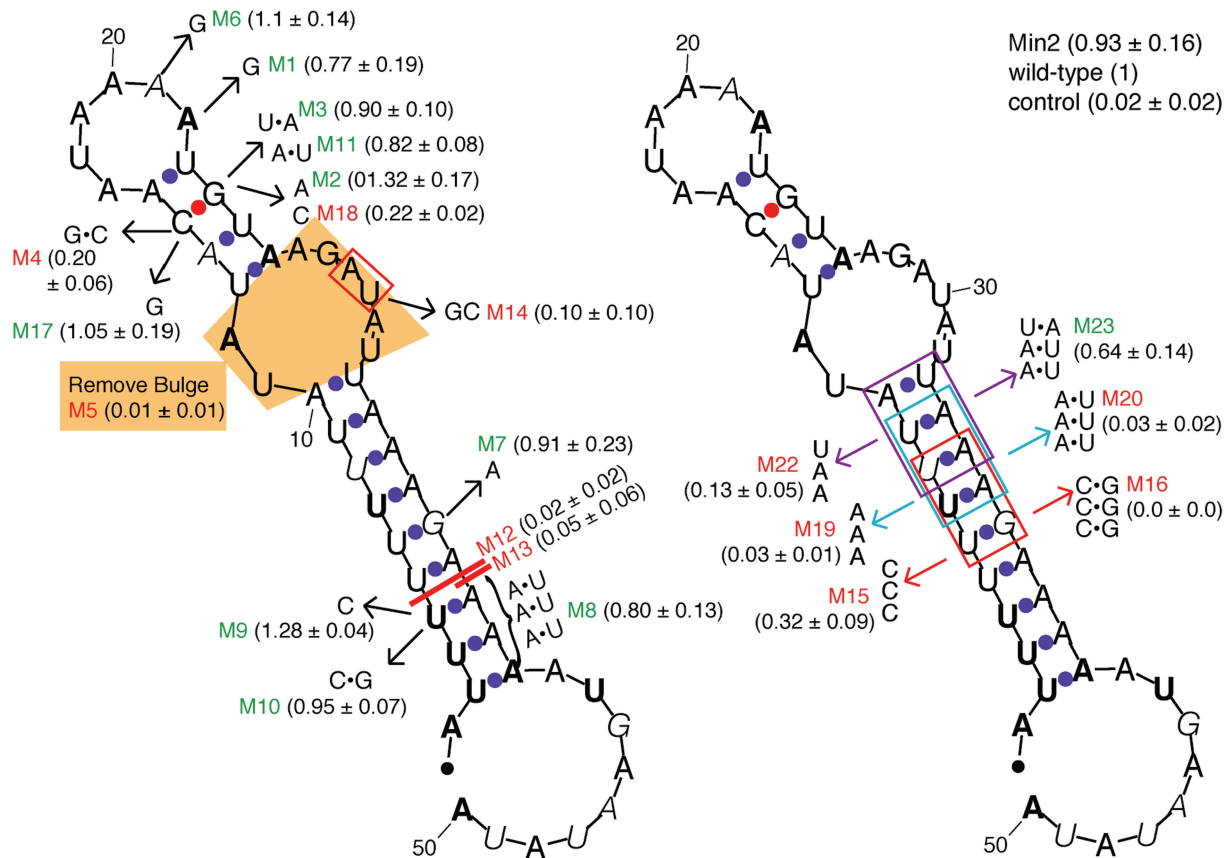
Figure 5. Mutagenesis analysis of Min2. The sequence and predicted secondary structure (31,32) of Min2 are shown above. Active (green) and significantly impaired (red) mutants are shown. Activity values shown reflect the mean fraction of colonies surviving on glycerol medium relative to wild-type (pATP2 carrying the native 636 nt *ATP2* 3′ UTR); control is a 500 nt random sequence. Nucleotides 11, 12 and 27–32 (highlighted in orange) were deleted in mutant M5. Error values reflect the SD of three or more independent trials. Bold nucleotides are highly conserved among the 13 sequences subjected to MEME analysis. Italicized nucleotides are non-conserved.
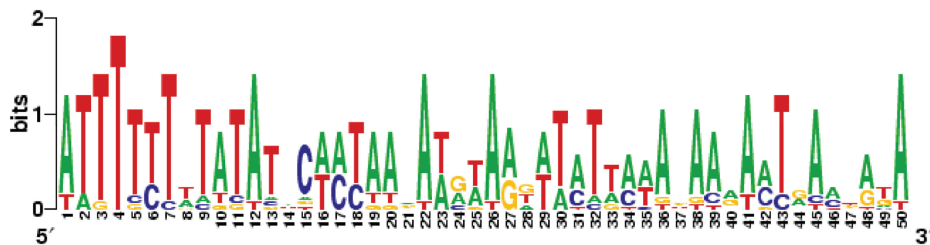
Figure 6. Sequence logo of Min2. The above sequence logo (created by weblogo.berkeley.edu) was generated from all 13 sequences used to discover the Min2 motif through MEME analysis (Table 2).

and qRT-PCR analyses (Figure 7). Quantitative RT–PCR analysis revealed approximately 4-fold differences in intracellular abundance; these differences may partially account for the observed changes in activity (Figure 7B). For example, M14 and the random 3′ UTR control are 50% as abundant as the wild-type 3′ UTR and their mitochondrial localization activities are reduced nearly 100-fold as judged by survival rates under selection conditions. Mutant M5, lacking the bulge of Min2, is only 25% as abundant as Min2, and its activity is 100-fold reduced compared with Min2. These results raise the possibility that the 3′ UTR expressed in the random

control and inactive mutants may destabilize the *ATP2* transcript, contributing to the loss of mRNA localization. To test this hypothesis, the mRNA degradation rates in *ATP2-3′ADH1* cells harboring pATP2-636, pAPT2-Min2 or pATP2-M5 were determined by treating cells with the RNA polymerase inhibitor thiolutin and measuring mRNA abundance by northern blot analysis (25). Over a period of 100 min, similar mRNA degradation rates were observed among the different clones (Figure 7C). In all cases tested, the *ATP2* transcript appears to be relatively stable over the course of 100 min, whereas the *ACT1* control mRNA degrades as expected over this
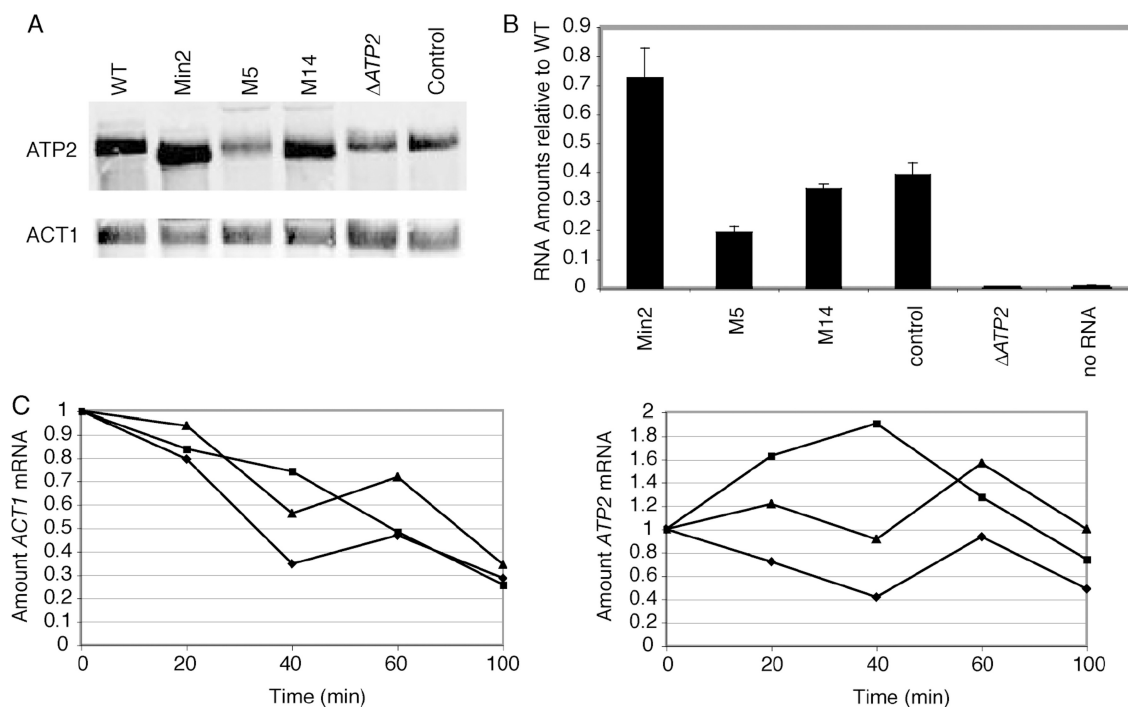
Figure 7. Analysis of *ATP2* mRNA expression. (**A**) Northern blot of poly(A) RNA probed with both *ATP2*-specific (top) and *ACT1*-specific (bottom) probes. WT = *ATP2* 636-nt 3′ UTR; Δ*ATP2* = *ATP2* ORF with *ADH1* 3′ UTR; Control = random 500 nt. (**B**) Quantitative RT-PCR analysis of mRNAs. Error bars represent SD of three or more independent trials. (**C**) *ACT1* and *ATP2* mRNA expression levels in a wild-type *ATP2* (diamonds) strain, or *ATP2-3′ADH1* strains bearing plasmid pATP2-Min2 (squares) or pATP2-M5 (triangles) were analyzed by northern blot over a period of 100 min. RNA amounts shown are relative to the amount of transcript measured at time 0.

period of time (25). These observations suggest that the 3′ UTRs expressed in the random control and inactive mutants do not negatively affect mRNA localization by destabilizing the *ATP2* transcript. Differences in intracellular abundance of the *ATP2* mRNA among mutants, however, may partially account for differences observed in their survival rates under selection conditions.

DISCUSSION

In this work, we describe the use of NRR and *in vivo* selection to functionally dissect the 3′ UTR of *ATP2*, one of ~100 mitochondrially targeted mRNAs that are encoded in the nucleus of yeast cells (16). Despite this large number of examples, little is understood about how this set of mRNAs translocates from the nucleus to the mitochondria, an activity that is essential for proper biogenesis of the cell. The ability of NRR to generate highly diversified libraries has been exploited to study the bud tip localization of *ASH1* (9), and to functionally dissect sRNAs and proteins in bacteria as well as *in vitro* evolved ribozymes (20–22). In this work, NRR led to the rapid identification of Min2, a minimal motif conserved among selection survivors that is a functional *cis*-element in localizing *ATP2* mRNA to the mitochondria. Min2 variants that are naturally present in the yeast genome were also identified. The region 263–312 nt downstream of the *ATP2* stop codon is also a functional element in our simple selection system for mitochondrial

mRNA localization, inducing a strong mRNA localization phenotype in both the glycerol and the gRNA assay.

A second region, between nt 164 and 213 downstream of the *ATP2* stop codon, is able to localize gRNA-particles to the mitochondria, but cannot fully rescue *ATP2-3′ADH1* cells growing on glycerol media. These results suggest that the region at nt 164–213 may be insufficient to allow the *ATP2* transcript to be optimally localized and to maintain the RNA in a state most conducive to co-translational import of Atp2p into the mitochondria (17,33,34). Corral-Debrinski and coworkers (17) similarly observed that a minimal 100 nt element, between 50 and 150 nt of the *ATP2* 3′ UTR, although able to target a reporter RNA to the mitochondria surface, was not sufficient, when expressed downstream of the *ATP2* stop codon, to fully rescue *ATP2-3′ADH1* cell growth on glycerol media. A more recent report by the same group suggests that for *SOD2* (a nuclear-encoded mitochondrial protein), both the 3′ UTR and an N-terminal mitochondrial-targeting sequence were needed to efficiently deliver an unrelated protein to the mitochondria (35).

Additionally, our initial attempts to localize GFP to the mitochondria by simply appending Min2 to the 3′ end of the GFP mRNA resulted in no mitochondrial localization of the protein as judged by fluorescence microscopy (data not shown). These results could indicate that the simple localization of the ORF of GFP mRNA to the mitochondria in this system is not sufficient to ensure the mitochondrial localization of GFP protein, or that Min2-mediated localization is context-dependent.

It should be noted that in our studies GFP was expressed from an *ADH1* promoter that drives the transcription of a highly abundant cytoplasmic protein; it is possible that cytoplasmic localization signals within the resulting 5′ UTR could favor cytoplasmic localization over mitochondrial targeting. Collectively, these findings suggest that context dependence results in the different behavior of minimized elements when fused to exogenous reporter mRNAs, and that multiple elements may exist in the *ATP2* transcript which synergistically contribute to localization of the *ATP2* mRNA and to the efficient translation and import of Atp2p.

Notably, Min2 is functional as an *ATP2* minimal localization element even though this element is distinct from previously identified active regions of the *ATP2* 3′ UTR. Corral-Debrinski and coworkers (17) previously demonstrated that a physiologically functional *ATP2* 3′ UTR consists of the first 250 nt directly following the *ATP2* stop codon. David and coworkers (36), moreover, recently mapped through DNA tiling arrays the end of the *ATP2* transcript to be at nt 253 after the stop codon. It is therefore unexpected that the region of the *ATP2* 3′ UTR that is most similar to Min2 (263–312 nt) lies outside the proposed transcribed region. Additional studies are needed to determine the generality of Min2-like sequences among the set of mRNAs localized to the mitochondria. Initial BLAST searches revealed that the Min2 sequence is naturally present in the 3′ UTR of at least one other nuclear-encoded mitochondrial gene, *FLX1* (84% sequence identity over a 32 nt stretch). It should be noted, however, that the BLAST search identifies primary sequence homology and our studies described below indicate that secondary structure is also an important component of mRNA localization. The original sequences identified through *in vivo* selection, for example, were often from the antisense strand of the *ATP2* gene, and it is possible that Min2 structural homologs present in natural UTRs lack sufficient sequence similarity to be detected by standard sequence homology searches.

The predicted structure of Min2 shows similarity to that of the 44 nt transport/localization sequence (TLS) found in the *Drosophila K10* mRNA, whose transport from nurse cells into the oocyte contributes to the establishment of dorsoventral polarity (37). The *K10* TLS, specifically, has an imperfect 17 bp stem (there are two 1 nt bulges on the 3′ side of the stem) that is highly AU-rich: 10 of the 17 nt on the 5′ end of the transcript are Us. In addition, this TLS contains an 8-base loop at the top of the stem, which is also AU-rich. Results from mutagenesis studies on the *K10* TLS bear similarities to those presented here. For example, altering the minor groove of the long AU-rich stem in the *K10* TLS was shown to impair localization activity (38). In our results, mutants that maintained the original Min2 structure but swapped UA pairs for AU or CG pairs exhibited similar losses in activity. Given these similarities, it is tempting to speculate that the mechanism by which *ATP2* mRNA is localized to the mitochondria may be general and conserved across different species.

The overall decrease in expression observed for the random 3′ UTR, M5 and M14 further suggests that a threshold for *ATP2* expression may need to be reached in order for cells to undergo proper mitochondrial biogenesis and that localization elements may affect not only transcript translocation, but other factors including mRNA stability, nuclear export and translation efficiency. In preliminary electrophoretic mobility shift assays (EMSA) with yeast whole cell extracts (WCE) and either Min2 or M5 RNA (the 50- or 42-mer), we observed that M5, in addition to decreasing *ATP2* expression, is also unable to productively bind to protein *trans*-factors. In contrast, Min2 can form specific macromolecular complexes with yeast WCE (data not shown). Collectively, these observations suggest that Min2-like motifs contribute to yeast mitochondria biogenesis in at least two ways: first, they help to maintain *ATP2* expression levels at a threshold sufficient to maintain respiratory-competent cells; second, they localize the transcript to the mitochondrial surface, likely through interactions with a *trans*-acting protein factor. Studies to use Min2 and its M5 mutant in experiments aimed at the identification and characterization of these *trans*-acting factors are underway.

REFERENCES

1. Gonsalvez,G.B., Urbinati,C.R. and Long,R.M. (2005) RNA localization in yeast: moving towards a mechanism. *Biol. Cell*, **97**, 75–86.
2. St Johnston,D. (2005) Moving messages: The intracellular localization of mRNAs. *Nat. Rev. Mol. Cell Biol.*, **6**, 363–375.
3. Long,R.M., Singer,R.H., Meng,X.H., Gonzalez,I., Nasmyth,K. and Jansen,R.P. (1997) Mating type switching in yeast controlled by asymmetric localization of ASH1 mRNA. *Science*, **277**, 383–387.
4. Takizawa,P.A., Sil,A., Swedlow,J.R., Herskowitz,I. and Vale,R.D. (1997) Actin-dependent localization of an RNA encoding a cell-fate determinant in yeast. *Nature*, **389**, 90–93.
5. Zahedi,R.P., Sickmann,A., Boehm,A.M., Winkler,C., Zufall,N., Schonfisch,B., Guiard,B., Pfanner,N. and Meisinger,C. (2006) Proteomic analysis of the yeast mitochondrial outer membrane reveals accumulation of a subclass of preproteins. *Mol. Biol. Cell*, **17**, 1436–1450.
6. Shepard,K.A., Gerber,A.P., Jambhekar,A., Takizawa,P.A., Brown,P.O., Herschlag,D., DeRisi,J.L. and Vale,R.D. (2003) Widespread cytoplasmic mRNA transport in yeast: Identification of 22 bud-localized transcripts using DNA microarray analysis. *Proc. Natl Acad. Sci. USA*, **100**, 11429–11434.

7. Takizawa,P.A., DeRisi,J.L., Wilhelm,J.E. and Vale,R.D. (2000) Plasma membrane compartmentalization in yeast by messenger RNA transport and a septin diffusion barrier. *Science*, **290**, 341–344.

8. Gonsalvez,G.B., Lehmann,K.A., Ho,D.K., Stanitsa,E.S., Williamson,J.R. and Long,R.M. (2003) RNA-protein interactions promote asymmetric sorting of the ASH1 mRNA ribonucleoprotein complex. *RNA*, **9**, 1383–1399.

9. Jambhekar,A., McDermott,K., Sorber,K., Shepard,K.A., Vale,R.D., Takizawa,P.A. and DeRisi,J.L. (2005) Unbiased selection of localization elements reveals cis-acting determinants of mRNA bud localization in Saccharomyces cerevisiae. *Proc. Natl Acad. Sci. USA*, **102**, 18005–18010.

10. Long,R.M., Gu,W., Lorimer,E., Singer,R.H. and Chartrand,P. (2000) She2p is a novel RNA-binding protein that recruits the Myo4p-She3p complex to ASH1 mRNA. *EMBO J.*, **19**, 6592–6601.

11. Olivier,C., Poirier,G., Gendron,P., Boisgontier,A., Major,F. and Chartrand,P. (2005) Identification of a conserved RNA motif essential for She2p recognition and mRNA localization to the yeast bud. *Mol. Cell. Biol.*, **25**, 4752–4766.

12. Takizawa,P.A. and Vale,R.D. (2000) The myosin motor, Myo4p, binds Ash1 mRNA via the adapter protein, She3p. *Proc. Natl Acad. Sci. USA*, **97**, 5273–5278.

13. Karlberg,E.O.L. and Andersson,S.G.E. (2003) Mitochondrial gene history and mRNA localization: is there a correlation? *Nat. Rev. Genet.*, **4**, 391–397.

14. Lithgow,T., Cuezva,J.M. and Silver,P.A. (1997) Highways for protein delivery to the mitochondria. *Trends Biochem. Sci.*, **22**, 110–113.

15. Margeot,A., Garcia,M., Wang,W., Tetaud,E., di Rago,J.P. and Jacq,C. (2005) Why are many mRNAs translated to the vicinity of mitochondria: a role in protein complex assembly? *Gene*, **354**, 64–71.

16. Marc,P., Margeot,A., Devaux,F., Blugeon,C., Corral-Debrinski,M. and Jacq,C. (2002) Genome-wide analysis of mRNAs targeted to yeast mitochondria. *EMBO Rep.*, **3**, 159–164.

17. Margeot,A., Blugeon,C., Sylvestre,J., Vialette,S., Jacq,C. and Corral-Debrinski,M. (2002) In Saccharomyces cerevisiae, ATP2 mRNA sorting to the vicinity of mitochondria is essential for respiratory function. *EMBO J.*, **21**, 6893–6904.

18. Anderson,J.S.J. and Parker,R. (2000) Computational identification of cis-acting elements affecting post-transcriptional control of gene expression in Saccharomyces cerevisiae. *Nucleic Acids Res.*, **28**, 1604–1617.

19. Bittker,J.A., Le,B.V. and Liu,D.R. (2002) Nucleic acid evolution and minimization by nonhomologous random recombination. *Nat. Biotechnol.*, **20**, 1024–1029.

20. Bittker,J.A., Le,B.V., Liu,J.M. and Liu,D.R. (2004) Directed evolution of protein enzymes using nonhomologous random recombination. *Proc. Natl Acad. Sci. USA*, **101**, 7011–7016.

21. Liu,J.M., Bittker,J.A., Lonshteyn,M. and Liu,D.R. (2005) Functional dissection of sRNA translational regulators by nonhomologous random recombination and in vivo selection. *Chem. Biol.*, **12**, 757–767.

22. Wang,Q.S. and Unrau,P.J. (2005) Ribozyme motif structure mapped using random recombination and selection. *RNA*, **11**, 404–411.

23. Sheff,M.A. and Thorn,K.S. (2004) Optimized cassettes for fluorescent protein tagging in Saccharomyces cerevisiae. *Yeast*, **21**, 661–670.

24. Campbell,R.E., Tour,O., Palmer,A.E., Steinbach,P.A., Baird,G.S., Zacharias,D.A. and Tsien,R.Y. (2002) A monomeric red fluorescent protein. *Proc. Natl Acad. Sci. USA*, **99**, 7877–7882.

25. Herrick,D., Parker,R. and Jacobson,A. (1990) Identification and comparison of stable and unstable messenger-RNAs in Saccharomyces cerevisiae. *Mol. Cell. Biol.*, **10**, 2269–2284.

26. Corral-Debrinski,M., Blugeon,C. and Jacq,C. (2000) In yeast, the 3′ untranslated region or the presequence of ATM1 is required for the exclusive localization of its mRNA to the vicinity of mitochondria. *Mol. Cell. Biol.*, **20**, 7881–7892.

27. Herrmann,J.M. and Funes,S. (2005) Biogenesis of cytochrome oxidase - Sophisticated assembly lines in the mitochondrial inner membrane. *Gene*, **354**, 43–52.

28. Bailey,T.L. and Elkan,C. (1994) Fitting a mixture model by expectation maximization to discover motifs in biopolymers. *Proceedings of the Second International Conference on Intelligent Systems for Molecular Biology*, AAAI Press, Menlo Park, California. pp. 28–36.

29. Crooks,G.E., Hon,G., Chandonia,J.M. and Brenner,S.E. (2004) WebLogo: a sequence logo generator. *Genome Res.*, **14**, 1188–1190.

30. Schneider,T.D. and Stephens,R.M. (1990) Sequence Logos – a new way to display consensus sequences. *Nucleic Acids Res.*, **18**, 6097–6100.

31. Zuker,M. (2003) Mfold web server for nucleic acid folding and hybridization prediction. *Nucleic Acids Res.*, **31**, 3406–3415.

32. Mathews,D.H., Sabina,J., Zuker,M. and Turner,D.H. (1999) Expanded sequence dependence of thermodynamic parameters improves prediction of RNA secondary structure. *J. Mol. Biol.*, **288**, 911–940.

33. Fujiki,M. and Verner,K. (1991) Coupling of protein-synthesis and mitochondrial import in a homologous yeast in vitro system. *J. Biol. Chem.*, **266**, 6841–6847.

34. Fujiki,M. and Verner,K. (1993) Coupling of cytosolic protein-synthesis and mitochondrial protein import in yeast – evidence for cotranslational import in vivo. *J. Biol. Chem.*, **268**, 1914–1920.

35. Kaltimbacher,V., Bonnet,C., Lecoeuvre,G., Forster,V., Sahel,J.A. and Corral-Debrinski,M. (2006) mRNA localization to the mitochondrial surface allows the efficient translocation inside the organelle of a nuclear recoded ATP6 protein. *RNA*, **12**, 1408–1417.

36. David,L., Huber,W., Granovskaia,M., Toedling,J., Palm,C.J., Bofkin,L., Jones,T., Davis,R.W. and Steinmetz,L.M. (2006) A high-resolution map of transcription in the yeast genome. *Proc. Natl Acad. Sci. USA*, **103**, 5320–5325.

37. Serano,T. and Cohen,R.S. (1995) A small predicted stem-loop structure mediates oocyte localization of Drosophila K10 messenger-RNA. *Development*, **121**, 3809–3818.

38. Cohen,R.S., Zhang,S. and Dollar,G.L. (2005) The positional, structural, and sequence requirements of the Drosophila TLS RNA localization element. *RNA*, **11**, 1017–1029.